# PCCP

CrossMark
click for updates

# A combined crossed molecular beam and theoretical investigation of the reaction of the *meta*-tolyl radical with vinylacetylene – toward the formation of methylnaphthalenes†

Tao Yang,[a] Lloyd Muzangwa,[a] Ralf I. Kaiser,*[a] Adeel Jamal[b] and Keiji Morokuma*[bc]

Crossed molecular beam experiments and electronic structure calculations on the reaction of the *meta*-tolyl radical with vinylacetylene were conducted to probe the formation of methyl-substituted naphthalene isomers. We present the compelling evidence that under single collision conditions 1- and 2-methylnaphthalene can be formed without an entrance barrier *via* indirect scattering dynamics through a bimolecular collision of two non-PAH reactants: the *meta*-tolyl radical and vinylacetylene. The electronic structure calculations, conducted at the UCCSD(T)-F12b/cc-pVDZ//UM06-2x/cc-pVTZ + ZPE(UM06-2x/cc-pVTZ) level of theory, reveal that this reaction is initiated by the barrierless addition of the *meta*-tolyl radical to the terminal vinyl carbon (C1) of vinylacetylene, *via* a van-der-Waals complex implying that this mechanism can play a key role in forming methyl-substituted PAHs in low temperature extreme environments such as the low temperature interstellar medium and hydrocarbon-rich atmospheres of planets and their moons in the outer solar system. The reaction mechanism, proposed from the $C_{11}H_{11}$ potential energy surface, involves a sequence of isomerizations involving hydrogen transfer and ring closure, followed by hydrogen dissociation, which eventually leads to 1- and 2-methylnaphthalene in an overall exoergic process.

## 1. Introduction

In recent decades, polycyclic aromatic hydrocarbons (PAHs) and their derivatives such as (partially) hydrogenated PAHs, substituted PAHs, and their cations have been regarded as key interstellar molecules due to their ubiquitous abundance in the interstellar medium (ISM).[1–3] Accounting for up to 20% of the interstellar carbon budget, PAH-related compounds (hydrogenated species, ionized species, clusters) were reported to be potential carriers of the unidentified infrared bands (UIBs)[1,4,5]

[a] *Department of Chemistry, University of Hawaii at Manoa, Honolulu, Hawaii 96822, USA. E-mail: ralfk@hawaii.edu; Tel: +1-808-956-5731*
[b] *Fukui Institute for Fundamental Chemistry, Kyoto University, Sakyo, Kyoto 606-8103, Japan. E-mail: morokuma@fukui.kyoto-u.ac.jp; Tel: +81-75-711-7843*
[c] *Department of Chemistry and Cherry L. Emerson Center for Scientific Computation, Emory University, Atlanta, Georgia 30322, USA*

† Electronic supplementary information (ESI) available: Table S1 gives the optimized geometries, and computed vibrational frequencies of the reactants, various intermediates, transition states and products of the reaction of *meta*-tolyl radical with vinylacetylene calculated at the UM06-2x/cc-pVTZ level of theory, Table S2 gives the forward and reverse RRKM rate constants (in $s^{-1}$) as functions of the collision energy $E$ (in kJ mol$^{-1}$) for the reaction steps from the reaction of *meta*-tolyl radical with vinylacetylene producing the initial adduct **i1**, and Table S3 gives the statistical product branching ratios (%) from the initial adduct **i1** as functions of the collision energy $E$ (in kJ mol$^{-1}$). See DOI: 10.1039/c5cp03285g

in the far-infrared (far-IR) region of the electromagnetic spectrum and of the diffuse interstellar bands (DIBs)[6–9] in the near-IR, visible and ultraviolet (UV) regions. These features are linked to the energy equilibration through UV absorption and IR emission as well as the ionization balance through the interaction with the electrons and ions in the interstellar medium.[1] Their spectroscopic signatures as well as the formation – destruction cycle of PAHs[10] might provide a detailed record of PAH evolution in the ISM. However, PAHs still remain mysterious not only in their precise spectroscopic assignments (not a single, individual PAH or its derivative has been assigned in the ISM),[7] but also their detailed formation and destruction mechanisms have remained elusive to date.[11]

In terrestrial environments, the environmental concerns of PAH emissions have increased dramatically, especially in the fast-developing counties.[12–14] Carbonaceous material represents one of the major classes of atmospheric aerosol particulate matters (PM) and is produced at an annual emission rate of nearly $10^8$ tons *via* the combustion of fossil fuels and biomass burning.[15] As toxic byproducts of the combustion processes, PAHs as present in fine particulate particles of sizes equal or below 2.5 μm are likely to be inhaled into lungs[16] and, therefore, are classified as carcinogenic[17–19] and mutagenic.[19,20] More complex PAHs of molecular weights above 500 amu are thought to be the

precursors of soot particles, whose annual production is estimated to be close to $10^7$ tons.[21] The absorption of PAHs and soot particles into soils and sediments can also dramatically change the bio-degradation rates of sediment-bound chemicals.[22] Furthermore, PAHs are considered as severe air and marine pollutants[23–25] that further contribute to the global warming.[26] Anthropogenic influences on the PAH emissions also require us to fully apprehend their formation and destruction mechanisms under combustion-like conditions.

The molecular growth processes initiated with the monocyclic structures including the phenyl radical ($C_6H_5$) and benzene ($C_6H_6$) are suggested to be important in PAH formation mechanisms.[27,28] Thereby, simple PAH species such as indene ($C_9H_8$) and naphthalene ($C_{10}H_8$) were generally proposed to be formed via the hydrogen abstraction-acetylene addition (HACA) mechanism (phenyl or phenyl-like radicals involved),[28–30] phenyl addition-cyclization (PAC) with unsaturated hydrocarbons[31–37] and cyclopentadiene (cyclopentadienyl) self-reactions.[38–40] Recent studies associated with phenyl radicals and unsaturated hydrocarbons allene ($C_3H_4$), methylacetylene ($C_3H_4$), 1,3-butadiene ($C_4H_6$) have clearly revealed that indene,[41,42] 1-methylindene ($C_{10}H_{10}$),[42] and 1,4-dihydro-naphthalene ($C_{10}H_{10}$)[42] can be formed in a high temperature chemical reactor under combustion-relevant conditions. For the first time, the facile formation of the naphthalene molecule through the reaction of the phenyl radical with acetylene ($C_2H_2$) in the chemical reactor further validates the HACA mechanism under combustion conditions.[43] In recent years, our group has also initiated a systematic investigation on PAH formation via the crossed beam reactions of the phenyl/phenyl-type (para-tolyl, $C_6H_4CH_3$) radicals with C3-, C4- and C5-unsaturated hydrocarbons under single collision conditions at collision energies of around 50 kJ mol$^{-1}$, and successfully identified indene (phenyl with allene/methylacetylene), naphthalene (phenyl with vinylacetylene ($C_4H_4$)), 1,4-dihydronaphthalene (phenyl with 1,3-butadiene), 2-methyl-naphthalene ($C_{11}H_{10}$, para-tolyl with vinylacetylene) and dimethyl-dihydronaphthalenes ($C_{12}H_{14}$, para-tolyl with isoprene ($C_5H_8$)). These exoergic reactions are initiated through the barrierless formation of van-der-Walls complexes via the phenyl/phenyl-like radicals addition, followed by isomerization such as cis/trans isomerization, hydrogen migration and cyclization, which eventually lead to the formation of bicyclic aromatic hydrocarbons accompanied by hydrogen losses. In this work, we present our crossed beam studies on the reaction of yet another phenyl-type radical – the meta-tolyl radical – with vinylacetylene to elucidate the formation of methylnaphthalenes in a single-collision event (Fig. 1). This de-facto barrierless reaction enables us to gain further insights on the synthesis of methyl-substituted PAHs in extreme environments (combustion flames and interstellar medium).

## 2. Experiment and theory

We studied the bimolecular gas phase reaction of meta-tolyl ($C_6H_4CH_3$; $X^2A_1$) with vinylacetylene ($H_2CCHCCH$; $X^1A'$) in a universal crossed molecular beam apparatus at the University of Hawai'i at Manoa.[44–47] The primary meta-tolyl radical beam
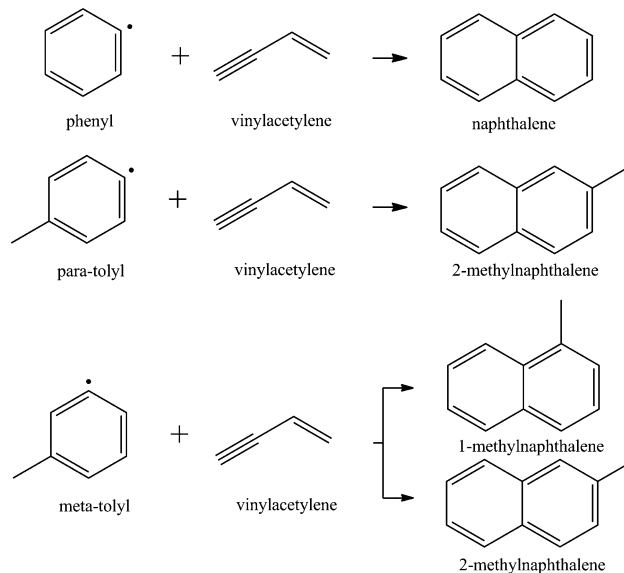


Fig. 1 Formation of (methyl-)naphthalenes via the crossed beam reactions of phenyl-type radicals (phenyl, para-tolyl, meta-tolyl) with vinylacetylene.

and the secondary vinylacetylene beam were generated in separate reactant chambers. In order to obtain the primary radical beam, helium gas at a pressure of 1.8 atm (99.9999%; Airgas Gaspro) was bubbled through the liquid meta-chlorotoluene precursor ($C_6H_4CH_3Cl$; 98%; Sigma-Aldrich) contained in a stainless steel bubbler; this mixture was then introduced into a piezo valve (Piezo Disk Translator; part number P-286.23; Physik Instrumente) operating at 120 Hz with pulses 80 µs. The helium seeded molecular beam of the chlorotoluene (0.1%) was then photolyzed by a spherically-focused 193 nm laser pulse of an 1 mm by 4 mm elliptical spot emitted from a Physik Compex 110 Excimer laser operating at 60 Hz and pulse energy of 18 ± 2 mJ. The supersonic beam containing the meta-tolyl radicals was then collimated by a skimmer of 1 mm diameter prior to entering the reaction chamber. A four-slot chopper wheel rotating at 120 Hz was located after the skimmer and selected a portion of the meta-tolyl radical beam with a well-defined peak velocity ($v_p$) and speed ratio ($S$) (Table 1). In the secondary reactant chamber, a pulsed molecular beam of 5% vinylacetylene seeded in argon gas (99.9999%; Airgas Gaspro) released at a backing pressure of 550 Torr operating at 120 Hz and a duration of 80 µs was released. Since both reactant beams are pulsed and have different velocities, we had to optimize the time delay to allow maximum overlap of the pulsed and hence optimum scattering signal. Here, the secondary beam was triggered 40 µs after the primary beam, while the laser was triggered 170 µs after the primary beam.

Table 1 Primary and secondary beam peak velocities ($v_p$), speed ratios ($S$), collision energy ($E_c$) and center-of-mass angle ($\theta_{CM}$) for the reaction of meta-tolyl ($C_6H_4CH_3$; 91 amu) with vinylacetylene ($H_2CCHCCH$; 52 amu)

| Beam | $v_p$ (ms$^{-1}$) | $S$ | $E_c$ (kJ mol$^{-1}$) | $\theta_{CM}$ |
|---|---|---|---|---|
| meta-Tolyl | 1593 ± 15 | 8.3 ± 0.4 | | |
| Vinylacetylene | 611 ± 20 | 8.0 ± 0.8 | 48 ± 3 | 12.3 ± 0.4 |

This journal is © the Owner Societies 2015

Phys. Chem. Chem. Phys., 2015, **17**, 21564–21575 | **21565**

We then recorded reactive scattering signal exploiting a triply differentially pumped quadruple mass spectrometer coupled to a Daly-type detector. The neutral products were initially ionized in the ionizer at an emission current of 2 mA and an electron energy of 80 eV. The ions of the desired mass-to-charge ($m/z$) then pass through the Extrel QC 150 quadrupole mass spectrometer before they are accelerated to the aluminum coated stainless steel cathode operating at $-22.5$ kV. The electron cascade is then repelled toward an aluminum-coated organic scintillator eventually initiating a photon cascade, which is detected by a Burle photomultiplier tube (Model 8850) and a Stanford Research System SR430 multichannel scalar with a discrimination level of 1.6 mV. We collected, integrated and normalized angular-resolved time-of-flight (TOF) spectra, and extracted the laboratory angular-dependent distribution at specific $m/z$ ratios. We further extracted on the scattering dynamics employing a forward-convolution routine to obtain two center-of-mass (CM) functions: the translational energy distribution $P(E_T)$ and the angular distribution $T(\theta)$.[48–50] The product flux contour map $I(\theta,u) = P(u) \times T(\theta)$ was generated to represent the differential cross section of the proposed reaction.[51]

To explore the $C_{11}H_{11}$ potential energy surface computationally in order to propose a reaction mechanism that leads to products, optimized geometries, vibrational frequencies, and zero-point vibration energies (ZPE) of reactants, intermediates, transition states, and products of the reaction of *meta*-tolyl radical with vinylacetylene were obtained using the hybrid density functional UM06-2x[54,55] with the correlation-consistent cc-pVTZ basis set[56,57] calculations. Vibrational frequency calculations with one imaginary frequency confirms that the stationary point is a transition state. Calculations of the intrinsic reaction coordinate (IRC) confirms that the transition state connects two intermediates. The optimized Cartesian coordinates of the reactants, intermediates, transition states, and products were used in single-point coupled cluster UCCSD(T)-F12b calculations[58,59] with the cc-pVDZ basis set; the E(UCCSD(T)-F12b/cc-pVDZ//UM06-2x/cc-pVTZ + ZPE(UM06-2x/6-cc-pVTZ)) energies are accurate within 10 kJ mol$^{-1}$ (Table S1, ESI†). To determine if there is a submerged

barrier that forms a van der Waals complex whose energy lies below the energy of the reactants, a relaxed potential energy scan of the reaction coordinate in 0.1 Å bond length increments between the separated reactants and the initial collision complex was performed at the UM06-2x/cc-pVTZ level of theory. Each optimized Cartesian coordinate was used in single-point E(UCCSD(T)-F12b/cc-pVDZ/UM06-2x/cc-pVTZ + ZPE(UM06-2x/6-cc-pVTZ)) calculations for consistency in computational methods used throughout this work. The GAUSSIAN 09[52] and MOLPRO 2012[53] programs were used for *ab initio* calculations. The forward and reverse energy-dependent rate constants $k(E)$ were obtained using the Rice–Ramsperger–Kassel–Marcus (RRKM) theory assuming the internal energy $E$ as a sum of the collision energy and the energy of the chemical activation. The density of states was computed within the harmonic approximation.[60] The micro-cannonical rate constants were then used in solving Ordinary Differential Equations (ODE) *via* the steady-state approximation, giving product branching ratios at different collision energies.[61] The optimized geometries, vibrational frequencies, forward and reverse rate constants, and product branching ratios are given in the ESI.†

## 3. Experimental results

Reactive scattering signal was searched at mass-to-charge ratios ($m/z$) of 143 ($C_{11}H_{11}^+$), 142 ($C_{11}H_{10}^+$), 141 ($C_{11}H_9^+$) and 128 ($C_{10}H_8^+$) for the reaction of *meta*-tolyl ($C_7H_7$; 91 amu) with vinylacetylene ($C_4H_4$; 52 amu). The TOF spectra at $m/z$ of 142, 141 and 128 depict identical pattern after scaling. This finding implies that signal at $m/z = 141$ and 128 originates from the dissociative ionization of the parent molecule ($C_{11}H_{10}$) in the electron impact ionizer of the detector. Also, within the signal-to-noise, TOFs at $m/z = 143$ also overlap with those at $m/z = 142$. This result implies that no $C_{11}H_{11}$ adduct is formed, and that signal at $m/z = 143$ originates from $^{13}CC_{10}H_{10}$. Further, we can conclude that only the *meta*-tolyl radical *versus* hydrogen atom exchange channel is open within this mass range, and that the
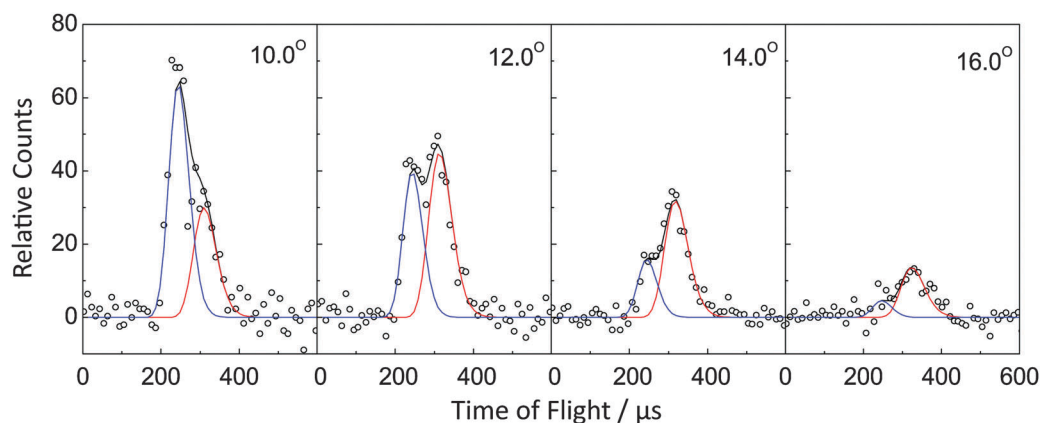


Fig. 2 Selected time-of-flight (TOF) spectra recorded at a mass-to-charge ratio ($m/z$) of 142 for the reaction of *meta*-tolyl with vinylacetylene. The circles present the experimental data, the red and blue lines represent the fit for the reactive and non-reactive scattering channel, respectively. The black solid lines represent the overall fit.
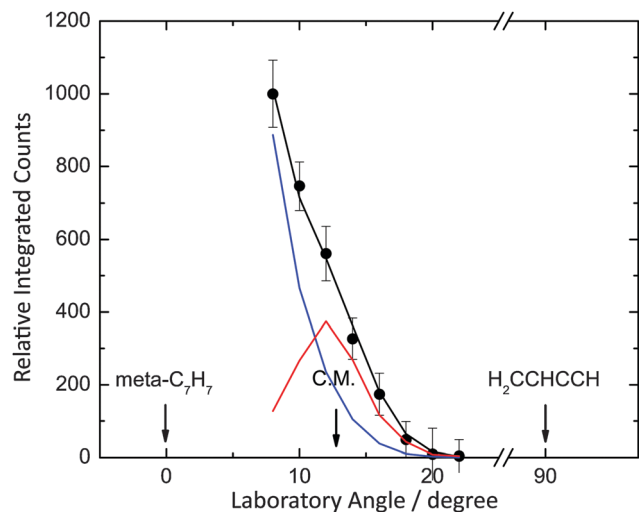
Fig. 3   Laboratory angular distribution for the reaction of *meta*-tolyl with vinylacetylene recorded at mass-to-charge ratio (*m/z*) of 142. The solid circles present the experimental data, the red and blue lines represent the fit for the reactive and non-reactive scattering channel, respectively. The black solid lines represent the overall fit.

molecular hydrogen and methyl group loss channels are closed. Accounting for the signal-to-noise ratio and data accumulation time, we recorded the TOF spectra of *m/z* = 142 at discrete angles from 8° to 22° in a step of 2°, and therefore obtained the respective laboratory angular distribution (Fig. 2 and 3).

A closer inspection of the TOF data suggests that the TOF spectra portray a bimodal profile holding two distinct maxima with the relative intensities of the two maxima differing significantly within the angular range. Further, the laboratory angular distribution revealed declining intensity from the angle closest to the primary beam down to 25°. This finding suggests that signal at *m/z* = 142 actually originates from two contributions: non-reactive scattering (fast component) and reactive scattering (slow component). To verify this postulate, we conducted a non-reactive scattering experiment between the species in the primary beam and a neat argon beam (secondary beam); recall that the secondary beam consists of a 5% mixture of vinyl-acetylene in argon gas. As a matter of fact, the decay profile of the laboratory angular distribution and the fast component of the TOFs could be nicely reproduced by non-reactive scattering signal from the primary beam, most likely due to the relatively low purity of the *meta*-chlorotoluene precursor of only 98%.

Therefore, to unveil the underlying reaction dynamics of the title reaction, we adopted a two-channel fit of the laboratory data in the forward-convolution routine to convert the laboratory data into two center-of-mass functions: the translational energy distributions $P(E_T)$s and angular distributions $T(\theta)$s (Fig. 4). Channel one (slow component, left column) accounted for the reactive scattering signal and exploited a reactant mass combination of 91 amu and 52 amu; the second channel (fast component, right column) was fit with a mass combination 142 amu and 40 amu thus simulating non-reactive scattering.
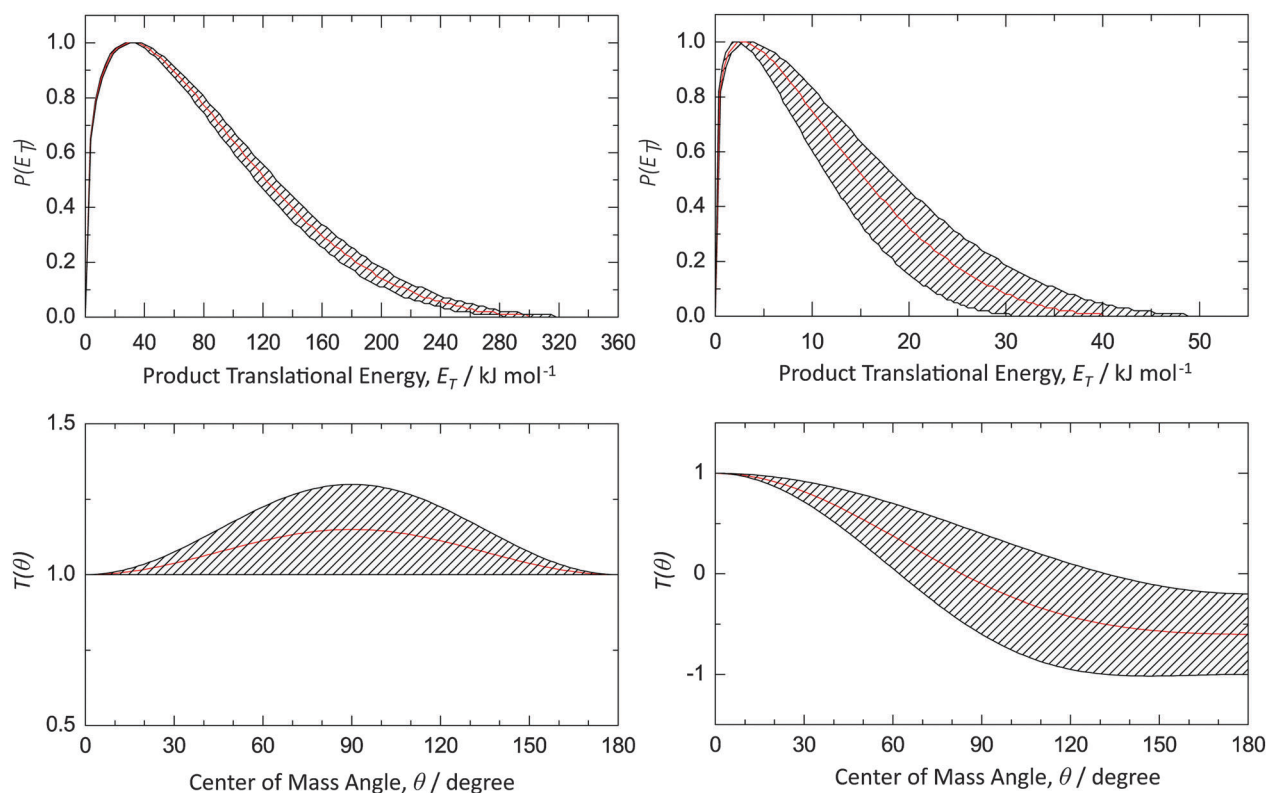


Fig. 4   Center-of-mass translational energy distributions $P(E_T)$s (top) and angular distributions $T(\theta)$s (bottom) in the reaction of *meta*-tolyl with vinylacetylene in the reactive scattering channel (left column) and the non-reactive scattering channel (right column), respectively. The hatched areas account for fits within the experimental error limits.
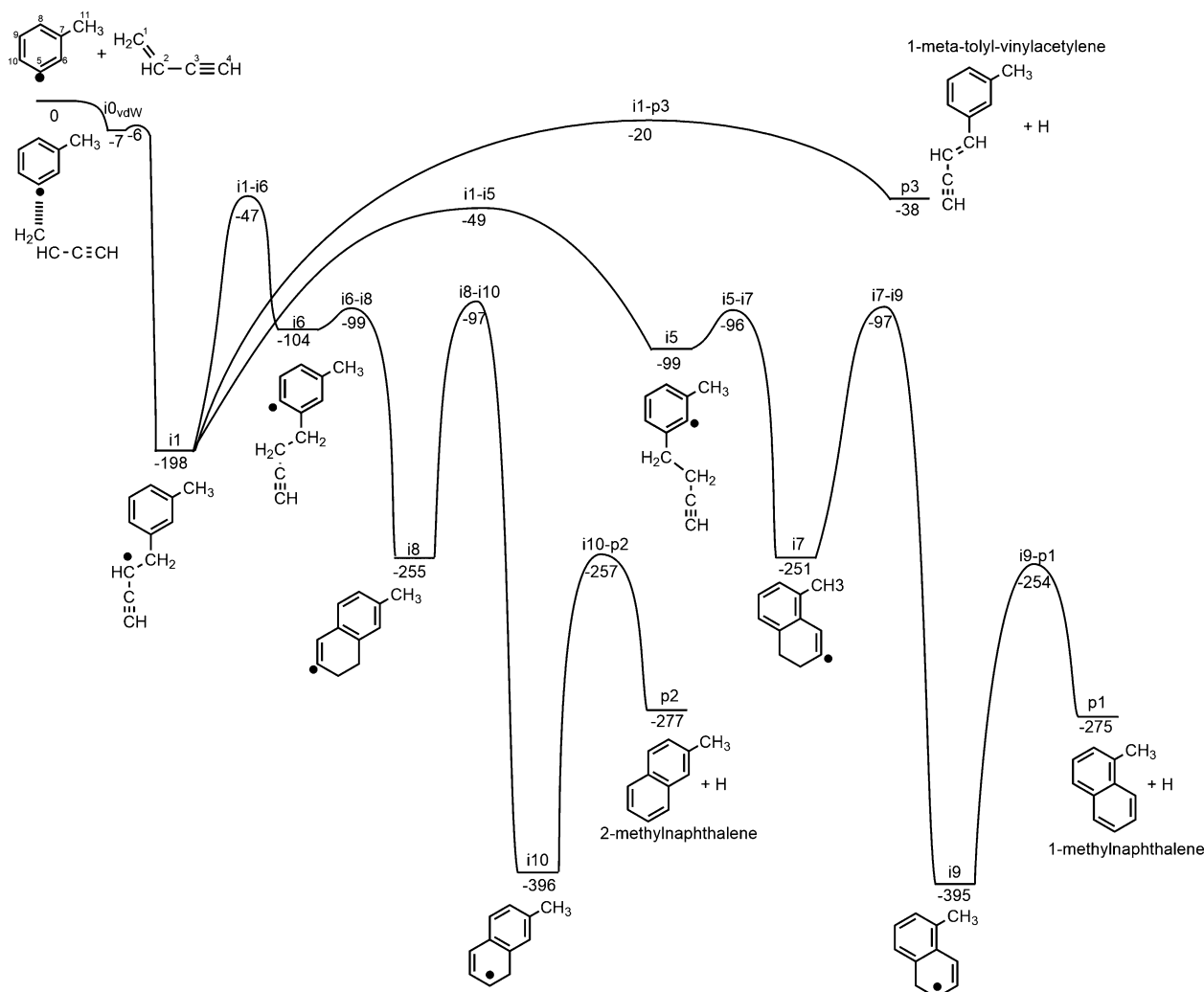
This journal is © the Owner Societies 2015

*Phys. Chem. Chem. Phys.*, 2015, **17**, 21564–21575 | **21567**

**Fig. 5** Proposed reaction mechanism based on stationary points on the $C_{11}H_{11}$ potential energy surface for the reaction of the *meta*-tolyl radical with C1 carbon of vinylacetylene. Energies for intermediates, transition states, and products are given relative to the reactants energy (in kJ mol$^{-1}$) at the at the UCCSD(T)-F12b/cc-pVDZ//UM06-2x/cc-pVTZ + ZPE(UM06-2x/cc-pVTZ) level of theory.

In the following section, we only focus on the analysis of the reactive scattering data. Considering the center-of-mass translational energy distribution, the $P(E_T)$ extends to a maximum translational energy as high as 299 ± 17 kJ mol$^{-1}$. For those molecules born without internal excitation, the high-energy cutoff presents the sum of the absolute energy of the reaction plus the collision energy; this allows us to determine the reaction to be exoergic by 251 ± 20 kJ mol$^{-1}$. Further, the $P(E_T)$ depicts a pronounced off-zero peaking between 20 and 40 kJ mol$^{-1}$; this finding implies the existence of a tight exit transition state and a repulsive energy release during the emission of the hydrogen atom.[62] Considering the principle of microscopic reversibility, an entrance barrier of this order-of-magnitude should exist for the reversed reaction, *i.e.* the addition of atomic hydrogen to a closed shell $C_{11}H_{10}$ hydrocarbon(s).[62] We also estimated the average energy channeling into the translational degrees of freedom to be 42 ± 3% of the total available energy proposing that the reaction product(s) is(are) likely formed *via* the indirect scattering dynamics.[63] Finally, we are analyzing the center-of-mass angular

distribution $T(\theta)$. Firstly, the $T(\theta)$ portrays flux over the complete angular range from 0° to 180° suggesting that the reaction of *meta*-tolyl with vinylacetylene involves indirect scattering dynamics upon the formation of bound $C_{11}H_{11}$ intermediate(s).[62] Secondly, the center-of-mass angular distribution depicts a pronounced maximum around 90°; this proposes that the hydrogen emission takes place almost parallel to the total angular momentum vector and nearly perpendicularly to the rotational plane of the decomposing complex(es) ('sideway scattering').[51] Lastly, the angular distribution is forward-backward symmetric with respect to 90°, indicating that the decomposing complex(es) has(have) a lifetime longer than its(their) rotational period(s).[64]

## 4. Computational results

The computational investigation revealed that the reaction of the *meta*-tolyl radical ($C_6H_4CH_3$; X$^2$A$_1$) with vinylacetylene ($H_2CCHCCH$; X$^1$A$'$) can take place *via* the addition of the

21568 | *Phys. Chem. Chem. Phys.*, 2015, **17**, 21564–21575

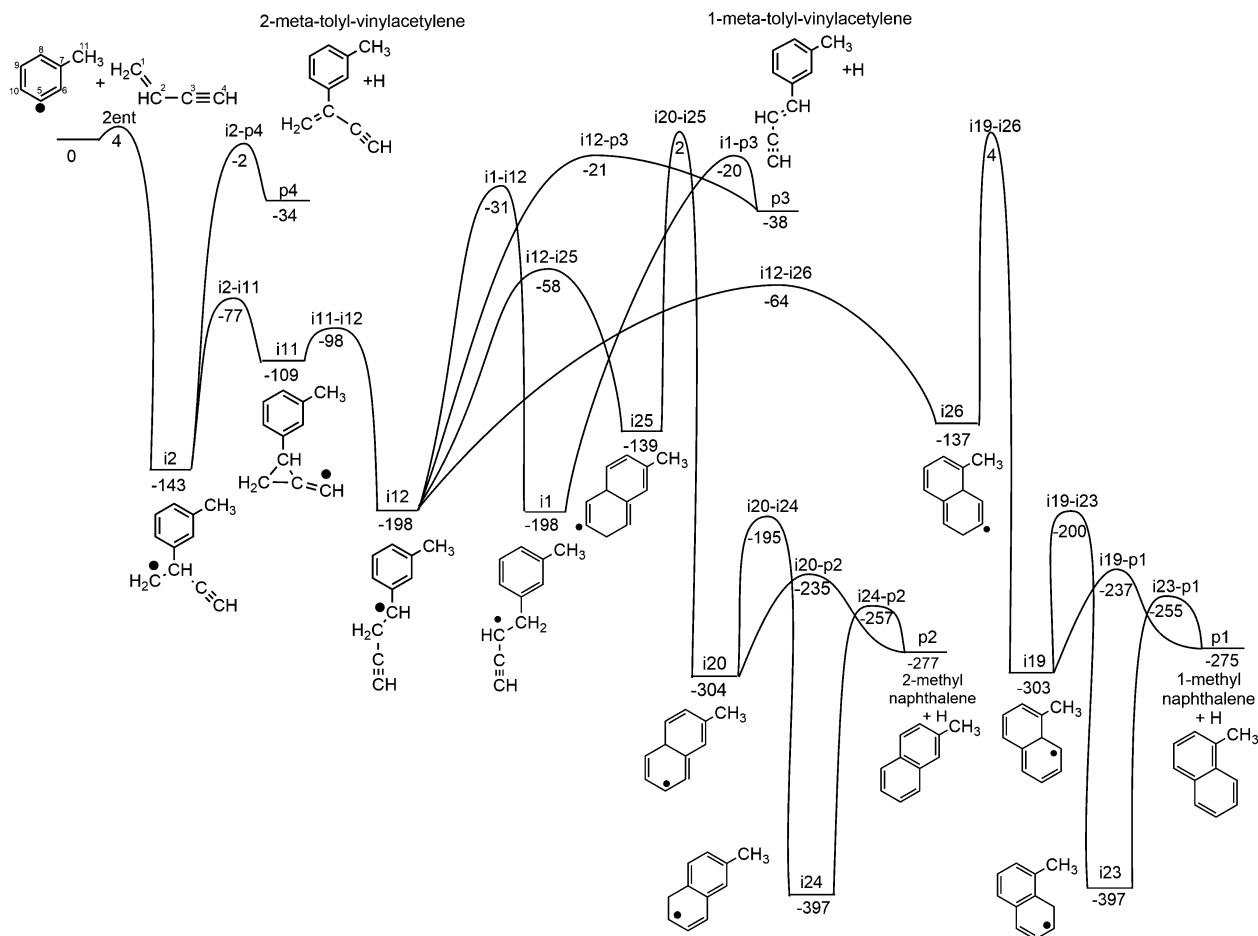This journal is © the Owner Societies 2015

**Fig. 6** Proposed reaction mechanism based on stationary points on the $C_{11}H_{11}$ potential energy surface for the reaction of the *meta*-tolyl radical with C2 carbon of vinylacetylene. Energies for intermediates, transition states, and products are given relative to the reactants energy (in kJ mol$^{-1}$) at the at the UCCSD(T)-F12b/cc-pVDZ//UM06-2x/cc-pVTZ + ZPE(UM06-2x/cc-pVTZ) level of theory.

*meta*-tolyl radical to any of the C1 to C4 carbon atoms of vinylacetylene; the reaction mechanisms that leads to products involve intermediates and the transition states connecting intermediates on the $C_{11}H_{11}$ potential energy surfaces (PESs) are illustrated in Fig. 5–8. Here, we present the energetically favorable channels leading to products.

The reaction pathway involving the addition of the *meta*-tolyl radical to the terminal vinyl carbon C1 of vinylacetylene (Fig. 5, with numeric labels) holds special distinction compared to the additions of C2 to C4 of vinylacetylene (Fig. 6–8). This addition proceeds without an entrance barrier *via* the formation of van-der-Waals complex **i0$_{vdW}$** residing in a shallow potential energy well of only 7 kJ mol$^{-1}$ with respect to the separated reactants. After overcoming a small barrier of only 1 kJ mol$^{-1}$, this complex isomerizes *via* addition of the *meta*-tolyl radical with its unpaired electron to the C1 atom of vinylacetylene forming the intermediate **i1** lying 198 kJ mol$^{-1}$ below the energy of the reactants. The succeeding reaction routes are divided into two general directions, one through the *ortho* pathway leading to 1-methylnaphthalene (**p1**, lying 275 kJ mol$^{-1}$ below the energy of the reactants), and the other through the *para* pathway leading to 2-methylnaphthalene (**p2**, lying 277 kJ mol$^{-1}$

below the energy of the reactants). For the *ortho* pathway, a 1,4-hydrogen migration from C6 to C2 can occur *via* transition state **TS$_{i1–i5}$** at a barrier height of 149 kJ mol$^{-1}$ relative to the energy of **i1**, leading to **i5** within the *ortho* tolyl framework. A cyclization between C4 and C6 of **i5** occurs *via* a low 3 kJ mol$^{-1}$ barrier height at **TS$_{i5–i7}$** relative to the energy of **i5**, leading to **i7**. Then, a 1,2 H-transfer from C3 to C2 occurs *via* transition state **TS$_{i7–i9}$** with a barrier height of 154 kJ mol$^{-1}$ relative to the energy of **i7**, leading to the resonantly stabilized free radical **i9**. Finally, a hydrogen atom dissociation from C1 of **i9** *via* transition state **TS$_{i9–p1}$** at a barrier height of 141 kJ mol$^{-1}$ leads to 1-methylnaphthalene. The *para* pathway follows a similar reaction mechanism as the *ortho* pathway, but involves the *para* C10 carbon oppose to the *ortho* C6 carbon. A 1,4-hydrogen migration from C10 to C2 occurs *via* transition state **TS$_{i1–i6}$** at a barrier height of 151 kJ mol$^{-1}$ relative to the energy of **i1**, to produce **i6** within *para* tolyl framework. Cyclization between C4 and C10 occurs *via* transition state **TS$_{i6–i8}$** at a barrier height of 5 kJ mol$^{-1}$ relative to the energy of **i6**, leading to **i8**. A 1,2 H-transfer from C3 and C2 of **i8** occurs *via* transition state **TS$_{i8–i10}$** at a barrier height of 158 kJ mol$^{-1}$ leading to **i10**. Finally, a hydrogen dissociation on C1 of **i10** occurs *via* transition state **TS$_{i10–p2}$** at a
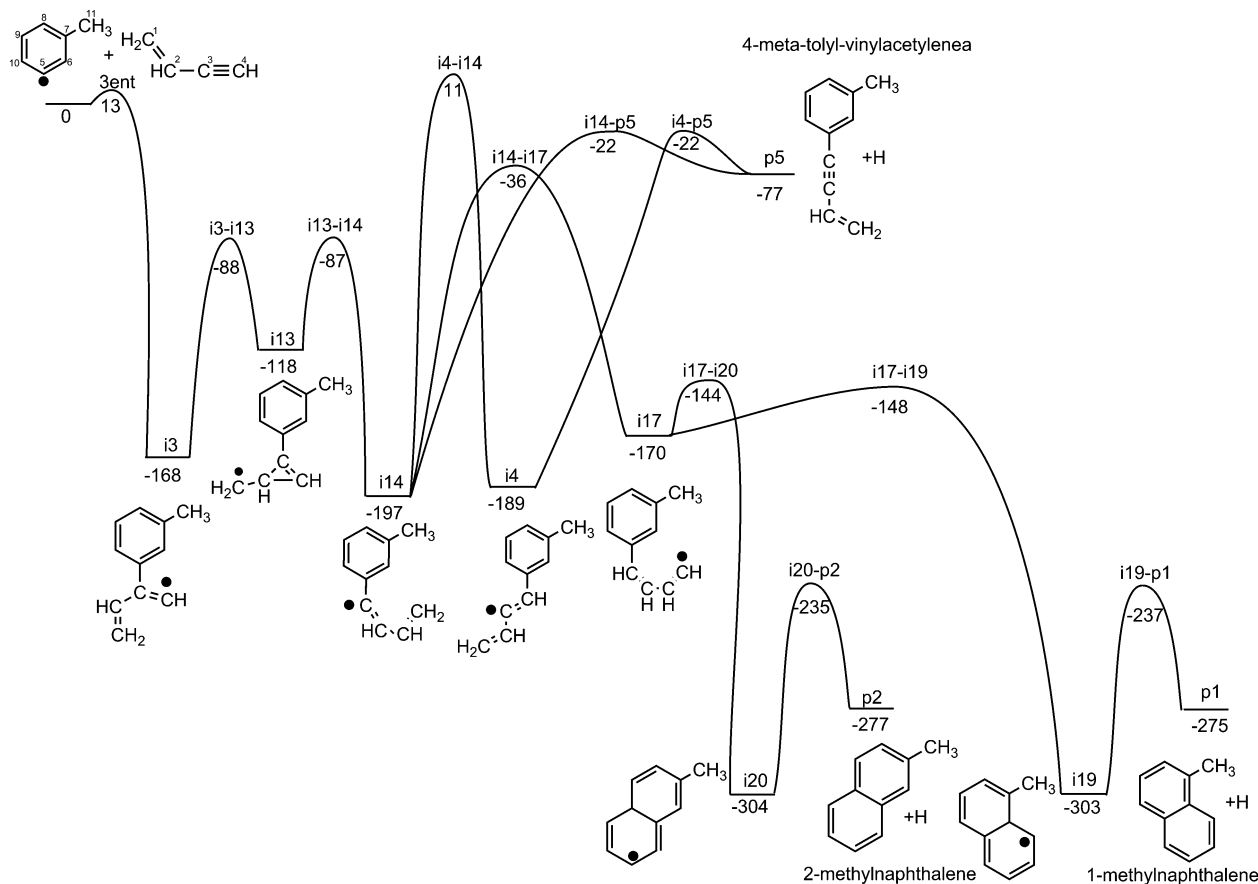
**Fig. 7** Proposed reaction mechanism based on stationary points on the $C_{11}H_{11}$ potential energy surface for the reaction of the *meta*-tolyl radical with C3 carbon of vinylacetylene. Energies for intermediates, transition states, and products are given relative to the reactants energy (in kJ mol$^{-1}$) at the at the UCCSD(T)-F12b/cc-pVDZ//UM06-2x/cc-pVTZ + ZPE(UM06-2x/cc-pVTZ) level of theory.

barrier height of 139 kJ mol$^{-1}$, leading to 2-methylnaphthalene. Alternatively, **i1** can dissociate a hydrogen atom from C1 to form 1-*meta*-tolyl-vinylacetylene (**p3**), residing 38 kJ mol$^{-1}$ below the energy of the reactants, *via* a transition state located 178 kJ mol$^{-1}$ above the energy of **i1**. An H-transfer from C1 to C2 of **i1** may also occur, leading to **i12** (Fig. 6), but the barrier height leading to **i12** (*via* transition state $TS_{i1-i12}$) is 18 kJ mol$^{-1}$ and 16 kJ mol$^{-1}$ higher than the barrier heights leading to **i5** (*via* transition state $TS_{i1-i5}$) and **i6** (*via* transition state $TS_{i1-i6}$), respectively.

The addition of *meta*-tolyl to the C2 carbon atom of vinylacetylene initiates the reaction pathway illustrated in Fig. 6. After overcoming an entrance barrier of 4 kJ mol$^{-1}$, intermediate **i2** is formed. This structure undergoes cyclization between C1 and C3 group yielding **i11**. A hydrogen dissociation from C2 of **i2** can occur, leading to 2-*meta*-tolyl-vinylacetylene (**p4**) lying 34 kJ mol$^{-1}$ below the energy of the reactants, but the barrier height leading to this product (*via* transition state $TS_{i2-p4}$) is 75 kJ mol$^{-1}$ higher than the cyclization process leading to **i11** (*via* transition state $TS_{i2-i11}$). A single bond rupture in the C2–C3 bond in **i11** leads through transition state $TS_{i11-i12}$ to the facile formation of **i12**. A hydrogen emission from C1 of **i12** can occur, yielding 1-*meta*-tolyl-vinylacetylene (**p3**), but the barrier height *via* transition state $TS_{i12-p3}$ leading to this product is 10 kJ mol$^{-1}$ higher in energy than the transition state $TS_{i1-i12}$

involving a 1,2 hydrogen transfer leading to **i1**. Alternatively, a C–C bond formation in the cyclization process between C4 and C6 or C10 in **i12** can occur, forming **i25** (*via* transition state $TS_{i12-i25}$) or **i26** (*via* transition state $TS_{i12-i26}$), respectively. Then, the transition states $TS_{i19-i25}$ and $TS_{i20-i26}$ involving a 1,2-hydrogen migration have energies that both lie above the energy of the reactants (4 kJ mol$^{-1}$ and 2 kJ mol$^{-1}$ respectively). Therefore, the reverse process, decyclization of **i25** and **i26** leading to back to **i12**, is the energetically favorable reaction route. As noted above, **i12** can isomerize to **i1**, which then encompasses the PES of the C1 pathways discussed with Fig. 5.

The PES for the addition of *meta*-tolyl radical to the C3 carbon of vinylacetylene is presented in Fig. 7. After passing an entrance barrier of 13 kJ mol$^{-1}$, the collision complex **i3** is formed. Once again, a cyclization occurs forming a three-membered ring, this time between C2 and C4 through transition state $TS_{i3-i13}$, leading to **i13**. A bond rupture between the C2 and C3 through transition state $TS_{i13-i14}$ leads to **i14**. This intermediate can follow a hydrogen dissociation from C4 *via* transition state $TS_{i14-p5}$ to yield 4-*meta*-tolyl-vinylacetylene (**p5**). However, an energetically favorable isomerization consisting of a 1,4-hydrogen transfer from C1 to C4 of **i14** can occur, leading to **i17** *via* transition state $TS_{i14-i17}$. Alternatively, a 1,2-hydrogen transfer from C3 to C4 in **i14** may also occur, but the energy of

**21570** | *Phys. Chem. Chem. Phys.*, 2015, **17**, 21564–21575
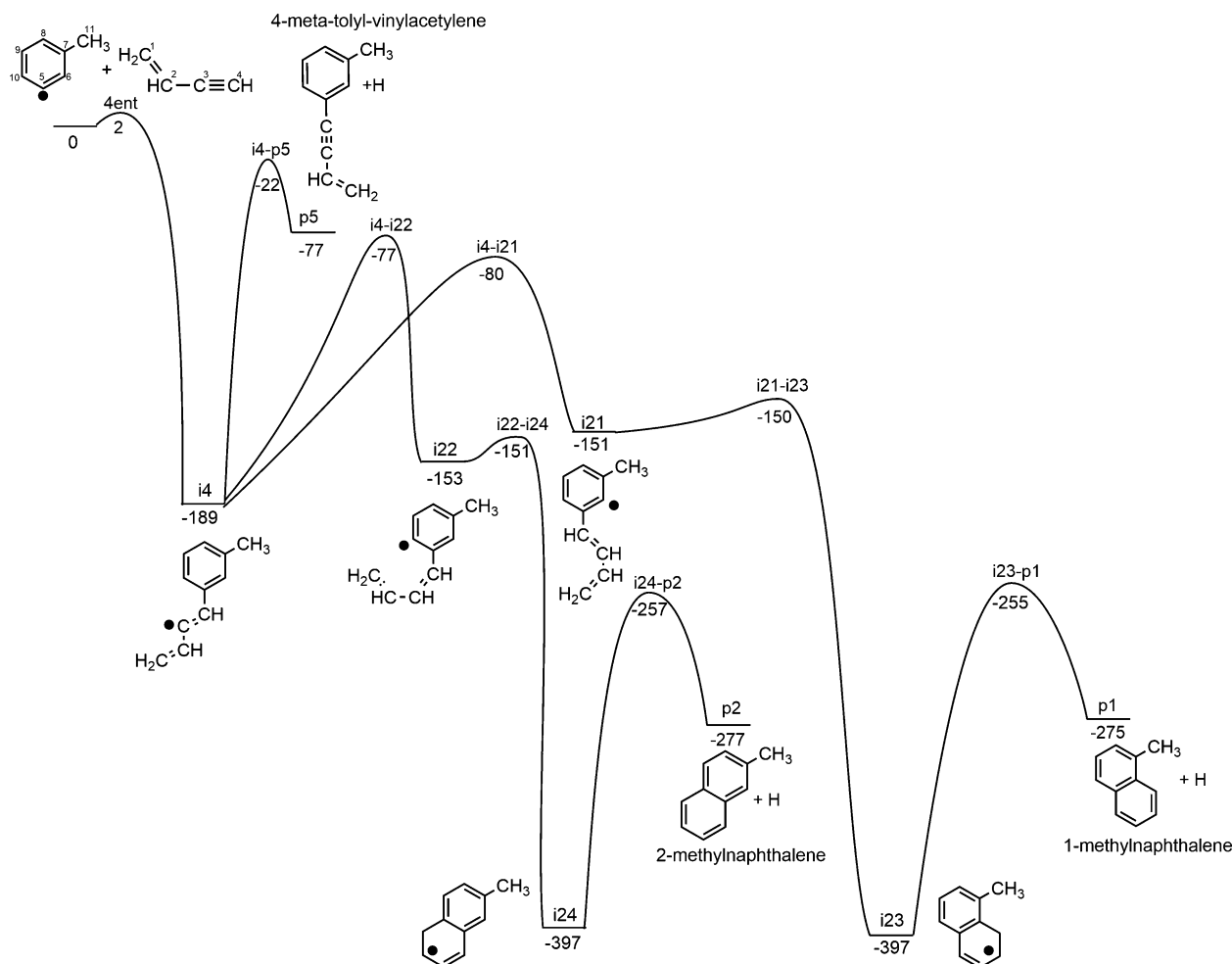
This journal is © the Owner Societies 2015

**Fig. 8** Proposed reaction mechanism based on stationary points on the $C_{11}H_{11}$ potential energy surface for the reaction of the *meta*-tolyl radical with C4 carbon of vinylacetylene. Energies for intermediates, transition states, and products are given relative to the reactants energy (in kJ $mol^{-1}$) at the at the UCCSD(T)-F12b/cc-pVDZ//UM06-2x/cc-pVTZ + ZPE(UM06-2x/cc-pVTZ) level of theory.

the barrier lies above the energy of the reactants (transition state **TS$_{i4–i14}$**). Finally, **i17** can form a C–C bond with C6 or C10, forming the resonantly stabilized radicals **i19** (*via* transition state **TS$_{i17–i19}$**) or **i20** (*via* transition state **TS$_{i17–i20}$**). A hydrogen dissociation from C6 of **i19** (*via* transition state **TS$_{i19–p1}$**) or C10 of **i20** (*via* transition state **TS$_{i20–p2}$**) leads to 1-methylnaphthalene and 2-methylnaphthalene, respectively.

Finally, the reaction pathway of the *meta*-tolyl radical addition to the C4 carbon of vinylacetylene is discussed (Fig. 8). The resonantly stabilized collision complex, **i4**, is formed by overcoming a low entrance barrier of 2 kJ $mol^{-1}$. Then, **i4** either decomposes through an atomic hydrogen loss channel *via* transition state **TS$_{i4–p5}$** to form 4-*meta*-tolyl-vinylacetylene (**p5**). However, a 1,4-hydrogen transfer from C6 to C3 of **i4**, facilitated by transition state **TS$_{i4–i21}$** leading to **i21**, is 58 kJ $mol^{-1}$ lower in energy than the exit barrier **TS$_{i4–p5}$**. Then **i21** can form a C–C bond between C1 and C6 through transition state **TS$_{i21–i23}$**, resulting in the resonantly stabilized **i23**. Finally, a hydrogen dissociation from C1 yields 1-methylnaphthalene (**p1**) *via* transition state **TS$_{i23–p1}$** *via* an exit barrier of about 20 kJ $mol^{-1}$. Similarly, a 1,4-hydrogen

transfer from C10 to C3 of **i4** through transition state **TS$_{i4–i22}$** leading to **i22** is 55 kJ $mol^{-1}$ lower in energy than the exit barrier **TS$_{i4–p5}$**. The intermediate **i22** can then go through a cyclization process through a C–C bond formation between C1 and C10 *via* transition state **TS$_{i22–i24}$**, leading to **i24**. Finally, C–H cleavage from C1 yields 2-methylnaphthalene (**p2**) through transition state **TS$_{i24–p4}$** *via* an exit barrier of 20 kJ $mol^{-1}$.

## 5. Discussion

We are now combining the experimental results with the electronic structure calculations to elucidate the underlying reaction mechanisms and chemical dynamics. Let us untangle the likely reaction product(s) first. The electronic structure calculations reveal five possible products formed in overall exoergic reactions: 1-methylnaphthalene (**p1**) at 275 kJ $mol^{-1}$, 2-methylnaphthalene (**p2**) at 277 kJ $mol^{-1}$, 1-*meta*-tolyl-vinyl-acetylene (**p3**) at 38 kJ $mol^{-1}$, 2-*meta*-tolyl-vinylacetylene (**p4**) at 34 kJ $mol^{-1}$, and 4-*meta*-tolyl-vinylacetylene (**p5**) at 77 kJ $mol^{-1}$.

A comparison with the experimental reaction exoergicity of $251 \pm 20$ kJ mol$^{-1}$ suggests at least 1-methylnaphthalene ($275 \pm 10$ kJ mol$^{-1}$) and/or 2-methylnaphthalene ($277 \pm 10$ kJ mol$^{-1}$) are formed. At the present stage, we cannot exclude that the thermodynamically less stable monocyclic isomers 1-*meta*-tolyl-vinyl-acetylene, 2-*meta*-tolyl-vinylacetylene and 4-*meta*-tolyl-vinylacetylene are also formed to a minor amount as well.

A closer look at the potential energy surfaces suggests that all pathways leading to the formation of 1-methylnaphthalene and 2-methylnaphthalene involve indirect scattering dynamics *via* long-lived C$_{11}$H$_{11}$ intermediate(s) as revealed from the shape of the center-of-mass angular distribution. In cold molecular clouds, where typical translational temperatures of 10 K prevail, only the barrierless formation of the van-der-Waals complex followed by addition to the C1 carbon atom *via* a submerged barrier leads to **i1**. The general reaction route leading to 1-methylnaphthalene from reactants involves **i1** → **i5** → **i7** → **i9** → 1-methylnaphthalene + H, while the general reaction route leading to 2-methylnaphthalene involves **i1** → **i6** → **i8** → **i10** → 2-methylnaphthalene + H. Furthermore, the **i1** → **i5** and **i1** → **i6** reaction steps involves a 1–4 hydrogen transfer from the aromatic ring to the C2 carbon of vinyl-acetylene, yielding a resonantly stabilized free radical on the aromatic ring. These reaction steps are energetically favorable over the competing exit channel of **i1** → 1-*meta*-vinylacetylene + H or any isomerization, including as **i1** → **i12**. The C–C bond forming ring-closure process occurs at a very low barrier height and re-establishes aromaticity on the ring. At elevated temperatures, the addition of the *meta*-tolyl radical to C2 and

C4 *via* moderate entrance barriers of 4 and 2 kJ mol$^{-1}$ leading to **i2** and **i4** may also be also feasible, respectively. For *meta*-tolyl addition to C4, a similar reaction mechanism leads to 1-methylnaphthalene + H and 2-methylnaphthalene + H, where, again, a 1,4-hydrogen transfer from C6 or C10 carbon occurs on the carbon adjacent to the addition site carbon, in this case C3 carbon.

It is important to highlight that all exit transition states, transition states: **TS$_{i9–p1}$**, **TS$_{i10–p2}$**, **TS$_{i19–p1}$**, **TS$_{i20–p2}$**, **TS$_{i23–p1}$**, **TS$_{i24–p2}$**, are computed to have non-zero exit barriers ranging from 21 kJ mol$^{-1}$ to 42 kJ mol$^{-1}$; this finding correlates nicely with the off-zero peaking of the center-of-mass translational energy distribution. Further, the hydrogen atoms are dissociated at dihedral angles with respect to the molecular plane of the decomposing intermediate of 99°, 88°, and 103° for transition states **TS$_{i9–p1}$**, **TS$_{i19–p1}$**, and **TS$_{i23–p1}$** for the formation of 1-methylnaphthalene, and 100°, 88°, and 100° for the transition states of **TS$_{i10–p2}$**, **TS$_{i20–p2}$**, and **TS$_{i24–p2}$** for the formation of 2-methylnaphthalene (Fig. 9). This prediction is in line with the experimental findings of the 'sideways' scattering as evident from the center-of-mass angular distribution. The calculated branching ratios are reported from the reaction routes leading to products from *meta*-tolyl radical addition to C1 of vinylacetylene. Therefore, only the reaction steps that lead to 1-methyl-naphthalene + H, 2-methyl-naphthalene + H, and 1-*meta*-tolyl-vinylacetylene + H are considered. The formation of 1-methyl-naphtalene + H in the 0–60 kJ mol$^{-1}$ collision energy range is 63.0–67.5%, while the 2-methyl-naphtalene + H branching ratio is 37.0–31.9% in the same collision range (Tables S2 and S3, ESI†). The formation
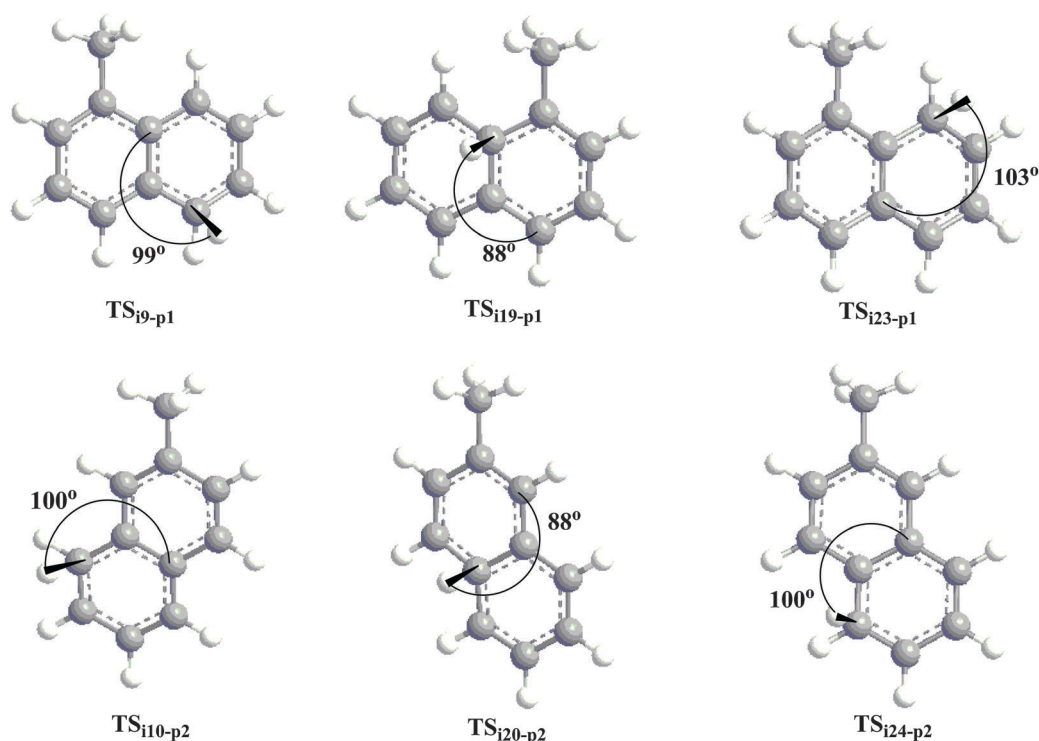


**Fig. 9** Computed dihedral angle between the molecular plane of the nascent 1-methylnaphthalene (top) and 2-methylnaphthalene (bottom) and dissociating H atom at the transition states from the intermediates **i9**, **i19**, and **i23** (top) to **i10**, **i20**, and **i24** (bottom).

of 1-*meta*-tolyl-vinylacetylene + H is negligible and accounts for the remainder product branching ratio. This is attributed to the slightly lower barrier height of the 1,4-hydrogen transfer from the *ortho* C6 carbon *versus* the *para* C10 carbon.

We would like to make comparison of the computed results for the present *meta*-tolyl radical reaction with vinylacetylene to the recently published results for *para*-tolyl radical reaction with vinylacetylene.[65] The most favorable reaction pathway for both reactions is initiated by forming a van-der-Waals complex on the terminal vinyl carbon atom (C1) of vinylacetylene, before the subsequent reactions take place through a submerged barrier for addition of *para*- and *meta*-tolyl radical and form *para*- and *meta*-tolyl-vinylacetylene adducts, respectively, with the radical center at the C2-position of the vinyl group. The subsequent reaction steps proceed with energies staying below those of the reactants, indicating that reactions of both *para*-tolyl and *meta*-tolyl with vinylacetylene can take place at very cold environment. For the *meta*-tolyl radical with vinylacetylene reaction, as seen in Fig. 5, the vinyl radical center of the initial adduct **i1** can abstract a hydrogen atom in two ways. One is abstraction of a hydrogen atom from C10 to form **i6**, which cyclizes to form **i8** and, after 1,2-hydrogen atom transfer and H-atom dissociation leads to the product 2-methylnaphthalene. The other is H abstraction from C8 to form **i5**, which cyclizes to form **i7** and, after 1,2-hydrogen atom transfer and H-atom dissociation, leads to the product 1-methylnaphthalene. In contrast, for *para*-tolyl radical with vinylacetylene reaction, the vinyl radical center of the initial adduct can abstract a hydrogen atom only in one way; abstraction of a hydrogen atom from the *meta*-tolyl position giving a resonantly stabilized free radical as an intermediate, which cyclizes and, after 1,2-hydrogen atom transfer and hydrogen atom loss, leads to the product 2-methylnaphthalene exclusively.

## 6. Conclusion

We conducted a crossed molecular beam study of *meta*-tolyl radicals with vinylacetylene at a collision energy of 48 kJ mol$^{-1}$. These experiments were merged with electronic structure and RRKM calculations of the $C_{11}H_{11}$ potential energy surface. Our investigation provided convincing evidence that two methyl-substituted PAHs – 1- and 2-methylnaphthalene – can be formed *via* indirect scattering dynamics through a bimolecular collision of two non-PAH reactants: the *meta*-tolyl radical and vinylacetylene. In low temperature environments such as in cold molecular clouds at 10 K, this reaction is initiated by the formation of a van-der-Waals complex followed by addition of the *meta*-tolyl radical to the vinyl (C1) carbon *via* a submerged barrier. The reaction mechanism based on the PES show that the energetically favorable reaction channel involves the formation of the initial collision complex or adduct and a 1,4-hydrogen transfer from the *ortho* or *para* carbon of tolyl radical to C2 of vinylacetylene. Then, a low barrier ring-closure process takes place, followed by a 1,2-hydrogen transfer, and finally dissociation of a hydrogen atom leading to 1-methylnaphthalene or 2-methylnaphthalene,

respectively. This barrierless route, addition to C1 of vinylacetylene yielding 1- and 2-methylnaphthalene, has strong implications to the formation of methyl-substituted PAHs in extreme environments such as in the interstellar medium and in hydrocarbon-rich atmospheres of planets and their moons in the outer Solar System. This experiment demonstrates a facile synthetic pathway to alkyl-substituted PAHs such as 1- and 2-methylnaphthalene in cold molecular clouds even at temperatures as low as 10 K potentially populating the interstellar medium with species responsible for the broad 3.4 μm feature in the unidentified infrared emission bands.

## References

1 A. G. Tielens, Interstellar polycyclic aromatic hydrocarbon molecules, *Annu. Rev. Astron. Astrophys.*, 2008, **46**, 289–337.

2 P. Ehrenfreund and M. A. Sephton, Carbon molecules in space: from astrochemistry to astrobiology, *Faraday Discuss.*, 2006, **133**, 277–288.

3 E. Dwek, Can composite fluffy dust particles solve the interstellar carbon crisis?, *Astrophys. J.*, 1997, **484**(2), 779.

4 K. Zhang, B. Guo, P. Colarusso and P. Bernath, Far-infrared emission spectra of selected gas-phase PAHs: spectroscopic fingerprints, *Science*, 1996, **274**(5287), 582–583.

5 L. Allamandola, A. Tielens and J. Barker, Polycyclic aromatic hydrocarbons and the unidentified infrared emission bands-Auto exhaust along the Milky Way, *Astrophys. J.*, 1985, **290**, L25–L28.

6 W. Duley, Polycyclic aromatic hydrocarbons, carbon nano-particles and the diffuse interstellar bands, *Faraday Discuss.*, 2006, **133**, 415–425.

7 P. J. Sarre, The diffuse interstellar bands: a major problem in astronomical spectroscopy, *J. Mol. Spectrosc.*, 2006, **238**(1), 1–10.

8 P. Ehrenfreund and S. B. Charnley, Organic molecules in the interstellar medium, comets, and meteorites: a voyage from dark clouds to the early Earth, *Annu. Rev. Astron. Astrophys.*, 2000, **38**(1), 427–483.

9 F. Salama, G. A. Galazutdinov, J. Krełowski, L. J. Allamandola and F. A. Musaev, Polycyclic Aromatic Hydrocarbons and the Diffuse Interstellar Bands: A Survey, *Astrophys. J.*, 1999, **526**, 265–273.

This journal is © the Owner Societies 2015

*Phys. Chem. Chem. Phys.*, 2015, **17**, 21564–21575 | 21573

10 J. Y. Seok, H. Hirashita and R. S. Asano, Formation history of polycyclic aromatic hydrocarbons in galaxies, *Mon. Not. R. Astron. Soc.*, 2014, **439**(2), 2186–2196.

11 Chemistry and physics of molecules and grains in space, *Faraday Discuss.*, 1998, **109**, 1–522.

12 M. Zheng, L. G. Salmon, J. J. Schauer, L. Zeng, C. Kiang, Y. Zhang and G. R. Cass, Seasonal trends in PM2. 5 source contributions in Beijing, China, *Atmos. Environ.*, 2005, **39**(22), 3967–3976.

13 H. Guo, S. Lee, K. Ho, X. Wang and S. Zou, Particle-associated polycyclic aromatic hydrocarbons in urban air of Hong Kong, *Atmos. Environ.*, 2003, **37**(38), 5307–5317.

14 M. del Rosario Sienra, N. G. Rosazza and M. Préndez, Polycyclic aromatic hydrocarbons and their molecular diagnostic ratios in urban atmospheric respirable particulate matter, *Atmos. Res.*, 2005, **75**(4), 267–281.

15 J. H. Seinfeld and J. F. Pankow, Organic atmospheric particulate material, *Annu. Rev. Phys. Chem.*, 2003, **54**(1), 121–140.

16 F. J. Miller, D. E. Gardner, J. A. Graham, R. E. Lee Jr, W. E. Wilson and J. D. Bachmann, Size considerations for establishing a standard for inhalable particles, *J. Air Pollut. Control Assoc.*, 1979, **29**(6), 610–615.

17 P. P. Fu, F. A. Beland and S. K. Yang, Cyclopenta-Polycyclic Aromatic-Hydrocarbons – Potential Carcinogens and Mutagens, *Carcinogenesis*, 1980, **1**(8), 725–727.

18 W. F. Busby, E. K. Stevens, E. R. Kellenbach, J. Cornelisse and J. Lugtenburg, Dose-Response Relationships of the Tumorigenicity of Cyclopenta[Cd]Pyrene, Benzo[a]Pyrene and 6-Nitrochrysene in a Newborn Mouse Lung Adenoma Bioassay, *Carcinogenesis*, 1988, **9**(5), 741–746.

19 K. H. Kim, S. A. Jahan, E. Kabir and R. J. C. Brown, A Review of Airborne Polycyclic Aromatic Hydrocarbons (PAHs) and their Human Health Effects, *Environ. Int.*, 2013, **60**, 71–80.

20 J. L. Durant, W. F. Busby, A. L. Lafleur, B. W. Penman and C. L. Crespi, Human Cell Mutagenicity of Oxygenated, Nitrated and Unsubstituted Polycyclic Aromatic Hydrocarbons Associated with Urban Aerosols, *Mutat. Res., Genet. Toxicol.*, 1996, **371**(3–4), 123–157.

21 Z. Mansurov, Soot formation in combustion processes (review), *Combust., Explos. Shock Waves*, 2005, **41**(6), 727–744.

22 A. L. C. Lima, J. W. Farrington and C. M. Reddy, Combustion-derived polycyclic aromatic hydrocarbons in the environment—a review, *Environ. Forensics*, 2005, **6**(2), 109–131.

23 K. J. Hylland, Polycyclic Aromatic Hydrocarbon (PAH) Eco-toxicology in Marine Ecosystems, *J. Toxicol. Environ. Health, Part A*, 2006, **69**, 109–123.

24 B. J. Finlayson-Pitts and J. N. Pitts Jr, Tropospheric Air Pollution: Ozone, Airborne Toxics, Polycyclic Aromatic Hydrocarbons, and Particles, *Science*, 1997, **276**, 1045–1052.

25 J. H. Seinfeld and J. F. Pankow, Organic Atmospheric Particulate Material, *Annu. Rev. Phys. Chem.*, 2003, **54**, 121–140.

26 R. J. Andres, T. A. Boden, F. M. Breon, P. Ciais, S. Davis, D. Erickson, J. S. Gregg, A. Jacobson, G. Marland, J. Miller, T. Oda, J. G. J. Olivier, M. R. Raupach, P. Rayner and K. Treanton, A Synthesis of Carbon Dioxide Emissions from Fossil-fuel Combustion, *Biogeosciences*, 2012, **9**(5), 1845–1871.

27 H. Richter and J. B. Howard, Formation of Polycyclic Aromatic Hydrocarbons and their Growth to Soot-A Review of Chemical Reaction Pathways, *Prog. Energy Combust. Sci.*, 2000, **26**(4–6), 565–608.

28 M. Frenklach, Reaction Mechanism of Soot Formation in Flames, *Phys. Chem. Chem. Phys.*, 2002, **4**(11), 2028–2037.

29 H. Wang and M. Frenklach, Calculations of Rate Coefficients for the Chemically Activated Reactions of Acetylene with Vinylic and Aromatic Radicals, *J. Phys. Chem.*, 1994, **98**(44), 11465–11489.

30 V. V. Kislov, N. I. Islamova, A. M. Kolker, S. H. Lin and A. M. Mebel, Hydrogen Abstraction Acetylene Addition and Diels–Alder Mechanisms of PAH Formation: A Detailed Study using First Principles Calculations, *J. Chem. Theory Comput.*, 2005, **1**(5), 908–924.

31 I. V. Tokmakov, J. Park and M. C. Lin, Experimental and Computational Studies of the Phenyl Radical Reaction with Propyne, *ChemPhysChem*, 2005, **6**(10), 2075–2085.

32 T. Yu and M. C. Lin, Kinetics of the Phenyl Radical Reaction with Ethylene – an RRKM Theoretical-Analysis of Low and High-Temperature Data, *Combust. Flame*, 1995, **100**(1–2), 169–176.

33 J. Park, G. J. Nam, I. V. Tokmakov and M. C. Lin, Experimental and Theoretical Studies of the Phenyl Radical Reaction with Propene, *J. Phys. Chem. A*, 2006, **110**(28), 8729–8735.

34 S. Fascella, C. Cavallotti, R. Rota and S. Carra, Quantum chemistry investigation of key reactions involved in the formation of naphthalene and indene, *J. Phys. Chem. A*, 2004, **108**(17), 3829–3843.

35 J. Park, S. Burova, A. S. Rodgers and M. C. Lin, Experimental and Theoretical Studies of the $C_6H_5 + C_6H_6$ reaction, *J. Phys. Chem. A*, 1999, **103**(45), 9036–9041.

36 M. Shukla, A. Susa, A. Miyoshi and M. Koshi, Role of phenyl radicals in the growth of polycyclic aromatic hydrocarbons, *J. Phys. Chem. A*, 2008, **112**(11), 2362–2369.

37 P. Lindstedt, L. Maurice and M. Meyer, Thermodynamic and kinetic issues in the formation and oxidation of aromatic species, *Faraday Discuss.*, 2001, **119**, 409–432.

38 D. Wang, A. Violi, D. H. Kim and J. A. Mullholland, Formation of naphthalene, indene, and benzene from cyclopentadiene pyrolysis: A DFT study, *J. Phys. Chem. A*, 2006, **110**(14), 4719–4725.

39 V. Kislov and A. Mebel, An *Ab Initio* G3-Type/Statistical Theory Study of the Formation of Indene in Combustion Flames. II. The Pathways Originating from Reactions of Cyclic C5 Species Cyclopentadiene and Cyclopentadienyl Radicals, *J. Phys. Chem. A*, 2008, **112**(4), 700–716.

40 N. Marinov, W. Pitz, C. Westbrook, M. Castaldi and S. Senkan, Modeling of aromatic and polycyclic aromatic hydrocarbon formation in premixed methane and ethane flames, *Combust. Sci. Technol.*, 1996, **116**(1–6), 211–287.

41 F. Zhang, R. I. Kaiser, V. V. Kislov, A. M. Mebel, A. Golan and M. Ahmed, A VUV photoionization study of the formation of the indene molecule and its isomers, *J. Phys. Chem. Lett.*, 2011, **2**(14), 1731–1735.

42 A. Golan, M. Ahmed, A. M. Mebel and R. I. Kaiser, A VUV Photoionization Study on the Multichannel Reaction of

Phenyl Radicals with 1,3-Butadiene under Combustion Relevant Conditions, *Phys. Chem. Chem. Phys.*, 2013, **15**, 341–347.

43 D. S. Parker, R. I. Kaiser, T. P. Troy and M. Ahmed, Hydrogen Abstraction/Acetylene Addition Revealed, *Angew. Chem., Int. Ed.*, 2014, **53**(30), 7740–7744.

44 Y. Guo, X. B. Gu, E. Kawamura and R. I. Kaiser, Design of a Modular and Versatile Interlock System for Ultrahigh Vacuum Machines: A Crossed Molecular Beam Setup as a Case Study, *Rev. Sci. Instrum.*, 2006, **77**(3), 034701.

45 X. B. Gu, Y. Guo, F. T. Zhang, A. M. Mebel and R. I. Kaiser, Reaction Dynamics of Carbon-bearing Radicals in Circumstellar Envelopes of Carbon Stars, *Faraday Discuss.*, 2006, **133**, 245–275.

46 R. I. Kaiser, P. Maksyutenko, C. Ennis, F. T. Zhang, X. B. Gu, S. P. Krishtal, A. M. Mebel, O. Kostko and M. Ahmed, Untangling the Chemical Evolution of Titan's Atmosphere and Surface-from Homogeneous to Heterogeneous Chemistry, *Faraday Discuss.*, 2010, **147**, 429–478.

47 F. T. Zhang, S. Kim and R. I. Kaiser, A Crossed Molecular Beams Study of the Reaction of the Ethynyl Radical ($C_2H(X^2\Sigma^+)$) with Allene ($H_2CCCH_2(X^1A_1)$), *Phys. Chem. Chem. Phys.*, 2009, **11**(23), 4707–4714.

48 J. D. Bittner, PhD thesis, Massachusetts Institute of Technology, Cambridge, MA 02139, USA, 1981.

49 P. S. Weiss, PhD thesis, University of California at Berkeley, Berkeley, California 94720, USA, 1986.

50 R. I. Kaiser, T. N. Le, T. L. Nguyen, A. M. Mebel, N. Balucani, Y. T. Lee, F. Stahl, P. V. Schleyer and H. F. Schaefer, A Combined Crossed Molecular Beam and *ab Initio* Investigation of $C_2$ and $C_3$ Elementary Reactions with Unsaturated Hydrocarbons – Pathways to Hydrogen Deficient Hydrocarbon Radicals in Combustion Flames, *Faraday Discuss.*, 2001, **119**, 51–66.

51 R. I. Kaiser, D. S. N. Parker, F. Zhang, A. Landera, V. V. Kislov and A. M. Mebel, PAH Formation under Single Collision Conditions: Reaction of Phenyl Radical and 1,3-Butadiene to Form 1,4-Dihydronaphthalene, *J. Phys. Chem. A*, 2012, **116**(17), 4248–4258.

52 M. Frisch, G. Trucks, H. B. Schlegel, G. Scuseria, M. Robb, J. Cheeseman, G. Scalmani, V. Barone, B. Mennucci and G. Petersson, *Gaussian 09, Revision A. 02*, Gaussian. Inc., Wallingford, CT, 2009, p. 200.

53 H. J. Werner, P. J. Knowles, G. Knizia, F. R. Manby and M. Schütz, Molpro: a general-purpose quantum chemistry program package, *Wiley Interdiscip. Rev.: Comput. Mol. Sci.*, 2012, **2**(2), 242–253.

54 Y. Zhao and D. G. Truhlar, The M06 suite of density functionals for main group thermochemistry, thermochemical kinetics, noncovalent interactions, excited states, and transition elements: two new functionals and systematic testing of four M06-class functionals and 12 other functionals, *Theor. Chem. Acc.*, 2008, **120**(1–3), 215–241.

55 E. Papajak, H. R. Leverentz, J. Zheng and D. G. Truhlar, Efficient Diffuse Basis Sets: cc-pV-x-Z + and maug-cc-pV-x-Z, *J. Chem. Theory Comput.*, 2009, **5**(5), 1197–1202.

56 T. H. Dunning Jr, Gaussian basis sets for use in correlated molecular calculations. I. The atoms boron through neon and hydrogen, *J. Chem. Phys.*, 1989, **90**(2), 1007–1023.

57 T. H. Dunning Jr, K. A. Peterson and A. K. Wilson, Gaussian basis sets for use in correlated molecular calculations. X. The atoms aluminum through argon revisited, *J. Chem. Phys.*, 2001, **114**(21), 9244–9253.

58 G. D. Purvis and R. J. Bartlett, A Full Coupled-Cluster Singles and Doubles Model – the Inclusion of Disconnected Triples, *J. Chem. Phys.*, 1982, **76**(4), 1910–1918.

59 G. Knizia, T. B. Adler and H.-J. Werner, Simplified CCSD (T)-F12 methods: Theory and benchmarks, *J. Chem. Phys.*, 2009, **130**(5), 054104.

60 V. V. Kislov, T. L. Nguyen, A. M. Mebel, S. H. Lin and S. C. Smith, Photodissociation of Benzene under Collision-free Conditions: An ab Initio/Rice–Ramsperger–Kassel–Marcus Study, *J. Chem. Phys.*, 2004, **120**(15), 7008–7017.

61 V. V. Kislov and A. M. Mebel, Ab Initio/RRKM-ME Study on the Mechanism and Kinetics of the Reaction of Phenyl Radical with 1,2-Butadiene, *J. Phys. Chem. A*, 2010, **114**(29), 7682–7692.

62 R. D. Levine, *Molecular Reaction Dynamics*, Cambridge University Press, Cambridge, UK, 2005.

63 R. I. Kaiser, Experimental Investigation on the Formation of Carbon-bearing Molecules in the Interstellar Medium via Neutral–neutral Reactions, *Chem. Rev.*, 2002, **102**(5), 1309–1358.

64 W. B. Miller, S. A. Safron and D. R. Herschbach, Exchange Reactions of Alkali Atoms with Alkali Halides: a Collision Complex Mechanism, *Faraday Discuss.*, 1967, **44**, 108–122.

65 D. S. N. Parker, B. B. Dangi, R. I. Kaiser, A. Jamal, M. N. Ryazantsev, K. Morokuma, A. Korte and W. Sander, An Experimental and Theoretical Study on the Formation of 2-Methylnaphthalene ($C_{11}H_{10}/C_{11}H_3D_7$) in the Reactions of the Para-Tolyl ($C_7H_7$) and Para-Tolyl-d7 ($C_7D_7$) with Vinylacetylene ($C_4H_4$), *J. Phys. Chem. A*, 2014, **118**, 2709–2718.

This journal is © the Owner Societies 2015

*Phys. Chem. Chem. Phys.*, 2015, **17**, 21564–21575 | **21575**